STRUCTURE OF LIGHT EXOTIC NUCLEI IN FERMIONIC MOLECULAR DYNAMICS

H. FELDMEIER, T. NEFF

Gesellschaft für Schwerionenforschung,
Planckstraße 1, 64291 Darmstadt, Germany

R. ROTH

Institut für Kernphysik, TU Darmstadt,
Schlossgartenstraße 9, 64289 Darmstadt, Germany

Helium and Beryllium isotopes are studied in the Fermionic Molecular Dynamics model. No a priori assumptions are made with respect to cluster structure or single-particle properties. An effective interaction based on the Argonne V18 interaction is used for all nuclei. Short-range central and tensor correlations are treated explicitly using a unitary correlation operator. Multiconfiguration calculations using the dipole and quadrupole moments as generator coordinates are able to describe the experimental binding energies and matter radii. The evolution of the cluster structure and the single-particle structure with increasing neutron number is discussed and predictions for yet unmeasured matter and charge radii are given.

1. Fermionic Molecular Dynamics

The A-body basis states in Fermionic Molecular Dynamics (FMD) [1] are parity and angular momentum projected Slater determinants $\left| Q \right\rangle$

$$\left| Q^{J^\pi}_{MK} \right\rangle = P^{J^\pi}_{MK} \left| Q \right\rangle , \tag{1}$$

of single particle states $\left| q_i \right\rangle$

$$\left| Q \right\rangle = \mathcal{A} \Big\{ \left| q_1 \right\rangle \otimes \ldots \otimes \left| q_A \right\rangle \Big\} . \tag{2}$$

The single-particle wave functions are described by Gaussian wave packets that are localized in phase-space

$$\left\langle \mathbf{x} \right| \left. q \right\rangle = \sum_i c_i \exp\left\{ -\frac{(\mathbf{x} - \mathbf{b}_i)^2}{2a_i} \right\} \left| \chi_i \right\rangle \otimes \left| \xi \right\rangle . \tag{3}$$

In contrast to the AMD approach [2] where the width parameter a is common to all wave packets FMD treats the width parameter as a complex variational parameter that can be different for each wave packet. Also the spins $\left|\,\chi\,\right\rangle$ of each wave packet are treated as variational parameters. A superposition of two Gaussian wave packets is used for each single-particle state $\left|\,q_i\,\right\rangle$.

The FMD many-particle state is determined by minimizing the intrinsic energy of the parity projected Slater determinant $\left|\,Q^{\pm}\,\right\rangle = \left|\,Q\,\right\rangle \pm \Pi \left|\,Q\,\right\rangle$

$$E\left[\left|\,Q^{\pi}\,\right\rangle\right] = \frac{\left\langle\, Q^{\pi}\,\right|\, H_{\mathit{eff}} - T_{cm} \left|\, Q^{\pi}\,\right\rangle}{\left\langle\, Q^{\pi}\,\right|\, Q^{\pi}\,\right\rangle} \tag{4}$$

with respect to all parameters of all single-particle states $\left|\,q_i\,\right\rangle$ defined in Eq. (3). After the minimization the many-particle state is projected on angular momentum. The correlation energy obtained by the projection can be very large for the often deformed and clustered nuclei in the p-shell. We therefore improve this projection after variation procedure (PAV$^{\pi}$) by implementing a variation after projection (VAP) procedure in the sense of the generator coordinate method (GCM). We minimize the energy of the Slater determinants under additional constraints on collective variables like radius, dipole, quadrupole or octupole moments. The VAP minimum can then be found by minimizing the projected energies with respect to the constraints. A further improvement is achieved by diagonalizing the Hamiltonian in a set of many-body states. This allows to study also excited states.

2. Effective interaction

For our calculations we use an effective interaction that is derived from the realistic Argonne V18 interaction by means of the Unitary Correlation Operator Method (UCOM) [3,4,5]. The correlated interaction includes the short-range central and tensor correlations induced by the repulsive core and the tensor force. The correlated interaction no longer connects to high momenta and can be used directly with the simple many-body states of a Hartree-Fock [5] or FMD approach. The contributions of three-body correlations and genuine three-body forces are simulated by an additional two-body correction term. This correction term consists of a central momentum dependent part that is adjusted to fix the saturation properties by fitting to the binding energies and radii of ^{4}He, ^{16}O, ^{40}Ca and a isospin dependent spin-orbit term that is fitted to the binding energies of ^{24}O, ^{34}Si

and ^{48}Ca. The correction term used in this paper differs slightly from the one in [5], as ^{16}O and ^{40}Ca are considered as tetrahedral α-cluster states that are about 5 MeV lower in energy after angular momentum projection than the spherical trial states. In total the correction term contributes about 15% to the potential energy.

3. Helium isotopes

Fig. 1 shows the one-body density of the intrinsic states $\left| Q \right\rangle$ obtained by minimizing the energy (4) of the Helium isotopes. In all nuclei a dipole deformation caused by a displacement of the neutrons against the α-core is found. In ^{6}He the configuration with two neutrons on the same side of the core is preferred to configurations with the two neutrons located at opposite sides of the core. In ^{8}He one approaches the $p_{3/2}$ neutron shell closure with an almost spherical neutron distribution but the displacement is still visible.

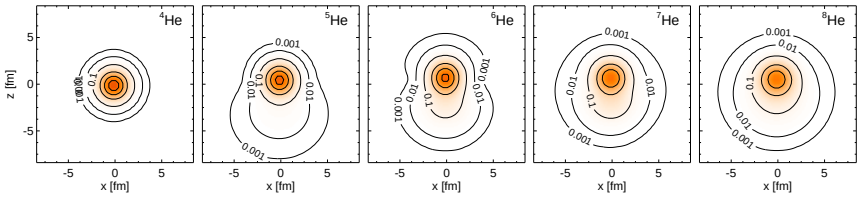

Figure 1. Intrinsic shapes of Helium isotopes corresponding to the variation after parity projection minima. Shown are cuts through the nucleon density calculated with the intrinsic state before parity projection. Densities are given in units of nuclear matter density $\rho_0 = 0.17\text{fm}^{-3}$.

In Fig. 3 the binding energies and matter radii obtained after angular momentum projection (PAV$^{\pi}$) are compared to the experimental binding energies and radii. To improve the many-body states we create additional configurations using the dipole moment as a generator coordinate, an example is shown in Fig. 2 for ^{6}He. The multiconfiguration calculations, i.e. diagonalizing the Hamiltonian in the many-body space spanned by these configurations, reproduce the experimental binding energies and radii very well (see Fig. 3). Hence, the borromean nature of ^{6}He and ^{8}He is explained by a correlated neutron cloud that sways against the α-core as a quantum zero-point oscillation of a soft-dipole mode.

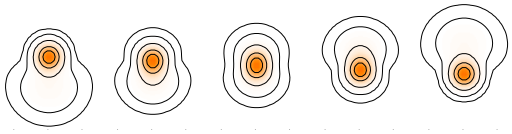

Figure 2. Typical configurations used for Multiconfig calculations of ^{6}He.

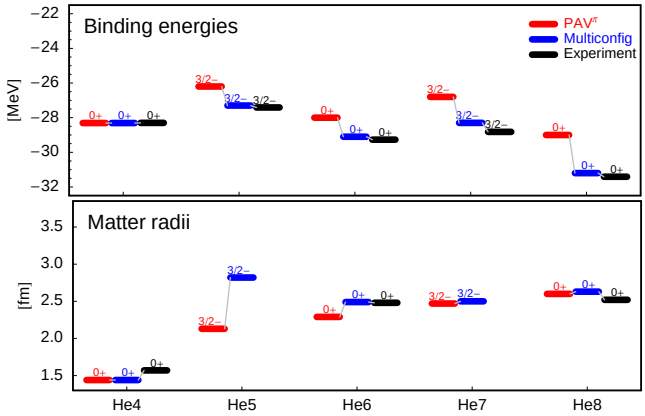

Figure 3. Binding energies and matter radii for the Helium isotopes. Results are given for the PAV$^\pi$ and the Multiconfig calculations. Experimental matter radii are taken from[6].

4. Beryllium isotopes

In Fig. 4 the intrinsic shapes of the Beryllium isotopes are shown. For ^{7}Be and ^{8}Be pronounced cluster structures can be seen and we find a strong similarity with Brink cluster wave-functions. In the heaver isotopes the α

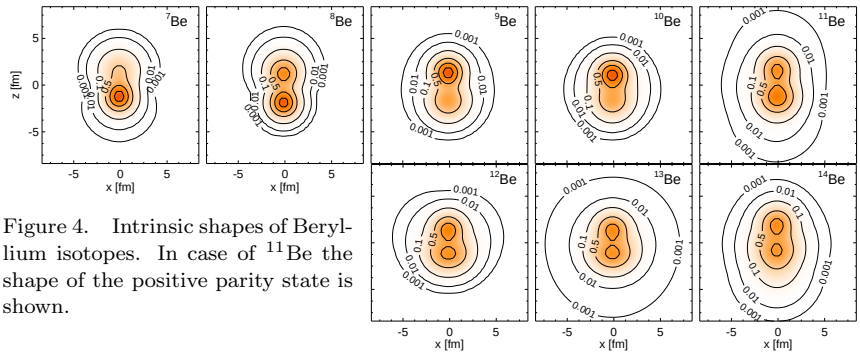

Figure 4. Intrinsic shapes of Beryllium isotopes. In case of ^{11}Be the shape of the positive parity state is shown.

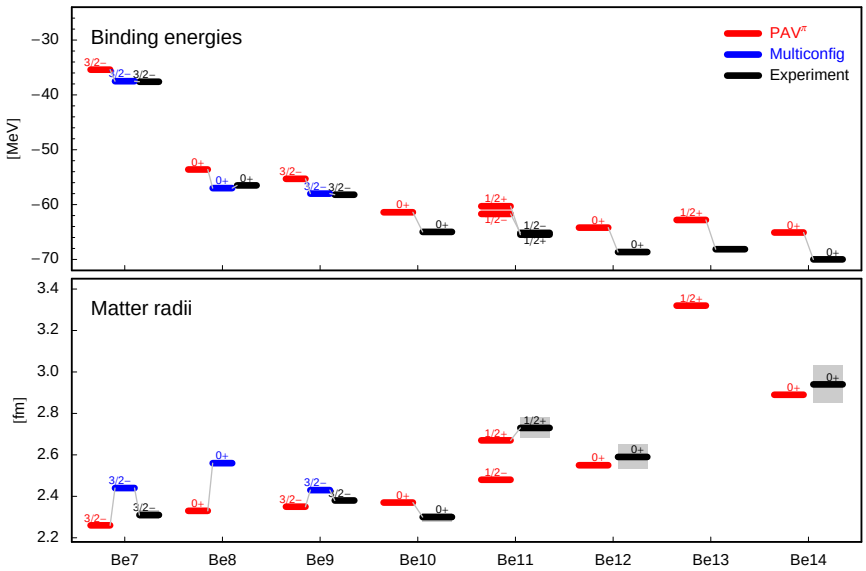

Figure 5. Energies and matter radii of Beryllium Isotopes. So far multiconfiguration calculations have only been done for ^{7}Be, ^{8}Be and ^{9}Be.

cluster structure survives but is modified by the additional neutrons. In ^{9}Be and ^{10}Be the additional neutrons seem to occupy the $p_{3/2}$ single-particle states. In experiment a parity inversion in ^{11}Be is observed. The $d_{5/2}$ single-particle states are coming down in energy and the $1/2^+$ groundstate is almost degenerate with the $1/2^-$ excited state. In the FMD PAV$^\pi$ calculations we find the $1/2^+$ state to be 1.5 MeV higher in energy than the $1/2^-$ state (see Fig. 5). The matter radius of the $1/2^+$ state is in good agreement with the experimental value. It has to be checked whether the level ordering will change in the multiconfiguration calculation. For the heavier ^{12}Be, ^{13}Be and ^{14}Be nuclei the $d_{5/2}$ and also the $1s_{1/2}$ single-particle states seem to be important. The general behaviour of ^{12}Be being bound, ^{13}Be being unbound and ^{14}Be being bound again as well as the matter radii are well reproduced, see Table 2.

5. Prediction of radii

Finally we summarize our predictions for the matter and charge radii in the following two tables. Matter radii are for point nucleons while the charge radii include the proton and neutron charge form factors.

Table 1. Matter and charge radii in fm for He isotopes

	r_{matter} [fm]			r_{charge} [fm]		
	PAV$^\pi$	Multiconfig	Exp[6]	PAV$^\pi$	Multiconfig	Exp
^{4}He	1.44		1.57±0.04	1.65		1.68
^{5}He	2.13	2.82		1.85	2.06	
^{6}He	2.28	2.49	2.48±0.03	1.93	2.02	2.054±0.014[7]
^{7}He	2.52	2.52		1.97	1.98	
^{8}He	2.60	2.63	2.52±0.03	1.97	1.99	

Table 2. Matter and charge radii in fm for Be isotopes. For ^{11,13}Be the $\frac{1}{2}^+$ states are used.

	r_{matter} [fm]			r_{charge} [fm]		
	PAV$^\pi$	Multiconfig	Exp[6]	PAV$^\pi$	Multiconfig	Exp
^{7}Be	2.26	2.44	2.31±0.02	2.47	2.64	
^{8}Be	2.33	2.56		2.47	2.68	
^{9}Be	2.35	2.43	2.38±0.01	2.41	2.50	2.52
^{10}Be	2.37		2.30±0.02	2.38		
^{11}Be	2.70		2.73±0.05	2.45		
^{12}Be	2.55		2.59±0.06	2.42		
^{13}Be	3.32			2.49		
^{14}Be	2.89		2.94±0.09	2.55		

References

1. H. Feldmeier and J. Schnack, Rev. Mod. Phys. **72** (2000) 655. and references therein
2. Y. Kanada-En'yo and H. Horiuchi, Prog. Theor. Phys. Suppl. **142** (2001) 205
3. H. Feldmeier, T. Neff, R. Roth, J. Schnack, Nuc. Phys. **A632** (1998) 61
4. T. Neff and H. Feldmeier, Nuc. Phys. **A713** (2003) 311
5. R. Roth, T. Neff, H. Hergert, H. Feldmeier, Nuc. Phys. **A745** (2004) 3
6. A. Ozawa, T. Suzuki and I. Tanihata, Nuc. Phys. **A693** (2001) 32
7. L.-B. Wang, P. Mueller, K. Bailey, G. W. F. Drake, J. P. Greene, D. Henderson, R. J. Holt, R. V. F. Janssens, C. L. Jiang, Z.-T. Lu, T. P. O'Connor, R. C. Pardo, K. E. Rehm, J. P. Schiffer, and X. D. Tang, Phys. Rev. Lett. **93** (2004) 142501